Molecular Science

AIMS Molecular Science, 12(4): 341–356.
DOI: 10.3934/molsci.2025020
Received: 30 April 2025
Revised: 24 September 2025
Accepted: 14 October 2025
Published: 21 October 2025

http://www.aimspress.com/journal/Molecular

Research article

Cationic nanocapsules as a non-viral vector for CRISPR-Cas9–based genome editing for myocilin associated glaucoma therapy

Karthikeyan Kesavan[1,*], Virendra Kumar[1], Jothimani Rajeswari[1], Charles Searby[2] and Val C. Sheffield[2]

[1] Department of Pharmacy, Guru Ghasidas Vishwavidyalaya (A Central University), Bilaspur, C.G., 495009, India
[2] Department of Pediatrics, Division of Medical Genetics and Genomics, Carver College of Medicine, University of Iowa, Iowa City, IA, 52242, USA

* **Correspondence:** Email: k7_76@rediffmail.com; dr.kkesavan@ggu.ac.in; Tel: +91-7587483123; Fax: +91 7752-260148.

Abstract: Our aim of this work was the development of positively charged D-α-tocopheryl glycol succinate 1000 (TPGS)-chitosan nanocapsules (TCNs) as a non-viral vector for effective genome editing. A two-step process was used to create cationic TCNs. TPGS was initially esterified using succinic anhydride to add a carboxylic acid group. Then, using a complex coacervation technique, ionic cross-linking was used to join the activated TPGS with chitosan. Fourier transform infrared (FTIR) spectroscopy was used to validate the synthesis of TCNs. A gel retardation experiment was performed to evaluate TCNs/pDNA complex entrapments at various N/P ratios (2:1, 5:1, and 10:1). The physicochemical properties of the TCNs/pDNA complex were identified. Plasmid DNA was protected from DNase I activity through TCN complexation. HEK293 and GTM3 cell lines were used to test *in vitro* transfection efficiency. At N/P 5:1, TCNs/pDNA exhibited the maximum transfection efficiency, which was comparable to Lipofectamine 3000™. Cellular uptake and localization studies confirmed effective delivery of Cas9-GFP plasmids using TCNs. A T7 endonuclease mismatch detection assay further demonstrated effective targeting and editing of the *MYOC* gene in HEK293 cells using our TCN delivery system. Based on these findings, cationic TCNs represent a promising non-viral gene delivery platform for potential treatment of myocilin-associated glaucoma.

Keywords: CRISPR; Glaucoma; Non-viral; Myocilin; Chitosan; TPGS

1. Introduction

The quality of life of patients can be greatly impacted by genetic disorders that affect eyesight, such as glaucoma [1]. Achieving optimal long-term gene expression through the effective transfer of genetic material to target cells is essential for successful gene therapy [2]. Despite the widespread use of viral vectors, the development of non-viral vectors is desirable due to the risks of viral vectors, which are mostly related to immunogenicity and mutagenesis [3]. A broad family of artificial complexes known as non-viral gene delivery systems is made up of a nucleic acid cargo, usually a plasmid, and a variety of soft materials, including lipids, surfactants, and synthetic and biological polymers [4].

Through the development of model organisms created by targeted modification and the repair of disease mutations for therapeutic purposes, clustered regularly interspaced short palindromic repeats (CRISPR) and CRISPR-associated (Cas) systems are potent tools for investigating and treating genetic disorders [5]. The Cas9-based gene editing platform has been delivered using physical techniques and viral vectors [6]. Non-viral vectors offer benefits over viral ones due to minimal immunogenicity and the lack of endogenous virus recombination, which may reduce the likelihood of both short-term and long-term negative consequences [7,8]. Additionally, compared to viral vectors, non-viral vectors are often simpler to synthesize and generate on a large scale, and they may be utilized to carry larger genetic payloads [9]. A successful gene delivery system should offer nano- or micro-sized structures to facilitate endocytosis or phagocytosis, shield the negatively charged phosphate nucleic acid backbone from anionic cell surface repulsion, and shield the nucleic acid from intracellular and extracellular nuclease degradation.

Juvenile open-angle glaucoma, an early-onset variant of primary open-angle glaucoma (POAG), has been demonstrated to be caused by mutations in the myocilin gene (*MYOC*) [10]. Myocilin-associated glaucoma is an excellent target for genome editing. The creation of many nano-/microcarriers as a result of various targeting property alterations has led to recent advancements in non-viral delivery methods [11]. Of these, cationic nanocarriers, which include cationic liposomes, polymers, dendrimers, and peptides, are most frequently employed in gene transfer as non-viral vectors [12–16]. They are made of positively charged lipids or polymers. Through electrical contact, cationic nanocarriers may load and condense nucleic acids due to their positively charged surface [12].

Several TPGS–chitosan–based delivery systems have been reported in the literature, primarily for drug delivery and ocular therapeutics. For example, TPGS–chitosan micelles have been explored for glaucoma therapy using brinzolamide, showing enhanced corneal penetration and sustained release [17]. Hybrid TPGS–chitosan nanocomposites have also been applied in oral drug delivery, improving solubility and bioavailability of poorly permeable drugs [18]. Similarly, TPGS–chitosan nanocapsules have been tested as antimicrobial or antifungal carriers [19]. However, to our knowledge, the application of TPGS–chitosan nanocapsules as non-viral vectors for genome editing has not been reported. We are the first to explore their potential as CRISPR/Cas9 delivery vehicles, specifically targeting *MYOC* gene editing for glaucoma therapy, thereby extending the use of this biocompatible system beyond conventional drug delivery.

2. Materials and methods

The chemicals used in this study were procured from Sigma-Aldrich Inc. (St. Louis, MO, USA). Low molecular weight chitosan (LMW) was obtained (Cat. No. 448869, CAS 9012-76-4), while D-α-Tocopherol polyethylene glycol 1000 succinate (TPGS) was purchased (Cat. No. 57668, CAS 9002-96-4). Succinic anhydride was supplied (Cat. No. 239690, CAS 108-30-5), and 4-(Dimethylamino)pyridine (DMAP) was procured (Cat. No. 107700, CAS 1122-58-3). Every chemical utilized was of commercial analytical quality and did not require additional purification. Gibco (Invitrogen, Thermo Fisher Scientific, Waltham, MA, USA) provided the Dulbecco's modified eagle medium (DMEM), foetal bovine serum (FBS), sodium pyruvate, penicillin streptomycin (PenStrep®), trypsine-DTA, and Opti-MEM.

2.1. Plasmids

The following plasmids were used in this study:

- pGFP reporter plasmid: Encoding enhanced green fluorescent protein (eGFP), purchased from Addgene (catalog no.64904). Throughout the manuscript, *pDNA* and *pGFP* are used interchangeably to refer to this plasmid.
- pSpCas9(BB)-2A-GFP (px458): A plasmid expressing SpCas9 and GFP, obtained from Addgene(catalog no. 48138).
- sgRNA–MYOC construct: An sgRNA targeting the *MYOC* locus (sequence: 5′-GTTCTTCTGTGCACGTTGC-3′) was cloned into the px458 backbone following the protocol of Jain et al. [10].

All plasmids were propagated in *E. coli* DH5α and purified using a commercial plasmid purification kit (Qiagen, catalog no.12943) prior to use in experiments.

2.2. Preparation of nanocapsules

2.2.1. Activation of TPGS

TPGS was initially esterified using succinic anhydride to functionalize it with a carboxylic acid group. To achieve this, 30 mL of anhydrous dichloromethane was used to dissolve 3.00g of pre-dried TPGS (1.95 mmol), 0.39g of succinic anhydride (3.90 mmol), and 0.24 g of 4-Dimethylaminopyridine (DMAP) (1.95 mmol). The mixture was stirred at 300 rpm under a nitrogen atmosphere at room temperature for 24 hours. To eliminate unreacted succinic anhydride, the product was dialyzed (Spectra/Por, MWCO 1000, U.S.A.) against 1:1 (v/v) water/ethanol for 72 hours after being precipitated in 20mL of cold diethyl ether [20,21].

2.2.2. TPGS-Chitosan Nanocapsules (TCN)

The polyelectrolyte complex coacervation technique was used to conjugate the carboxylic acid groups of TPGS with chitosan (Figure 1) [22]. To achieve this, 10mL of 1% glacial acetic acid were used to dissolve 7 mg of chitosan. Furthermore, 10 mL of distilled water were used to dissolve 14 mg of activated TPGS. Next, drops of the TPGS solution were added to the chitosan solution. A

magnetic stirrer was used to agitate the mixture at 400–600 rpm [23].

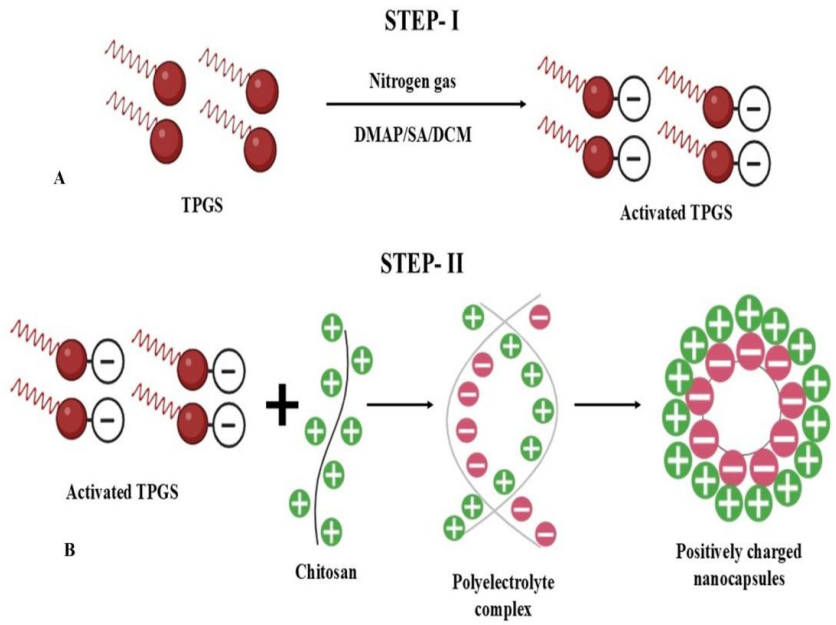

Figure 1: Schematic diagram of the synthesis process of TCNs. (A) TPGS was initially esterified using succinic anhydride to functionalize it with a carboxylic acid group. (B) The polyelectrolyte complex coacervation technique was used to conjugate the carboxylic acid groups of activated TPGS with an amine group of chitosan to form positively charged TCNs.

2.3. Complex formation of nanocarriers with plasmid DNA

After adding the proper quantity of TCNs to pGFP in N/P ratios (2:1, 5:1, and 10:1), the mixture was incubated for 20 minutes at room temperature [24].

2.4. Fourier transform infrared (FTIR) spectroscopy

The spectrum data of TPGS, TPGS-COOH, chitosan, and TCNs were recorded using a FTIR spectrophotometer (Bruker alpha spectrophotometer, USA). After preparing the sample pellets with KBr, they were scanned for transmittance using a 400–4000 cm^{-1} scanning range, with a fixed resolution of 2 cm^{-1}.

2.5. Electrophoretic mobility and enzymatic digestion assays

Gel electrophoresis was used to assess the electrophoretic mobility of the TCNs-pGFP complexes. In comparable TCNs-pGFP complexes with varying N/P ratios (2:1, 5:1, and 10:1), 100ng of pGFP (10 ng/μL) were combined with 4 μL of loading buffer, loaded onto agarose gels (1% w/v), and electrophoresed in TAE buffer at 6 V/cm for 60 minutes. After 15 minutes of SYBR Gold staining, the gels were visualized using a transilluminator [25]. The TCNs-pGFP complex was

electrophoresed on 1% agarose gels to evaluate pGFP encapsulation inside particles and protection from external DNase I. In short, 10 μL of an aqueous dispersion of TCNs-pGFP complex at various N/P ratios were loaded onto a gel after being incubated with 5 μL of DNase I (5 mg/mL in Tris solution) for 15–20 minutes at 4–8℃. The gel was also loaded with an identical volume of untreated TCNs containing the equivalent amount of pGFP. Free plasmid DNA (pGFP) served as a positive control [26].

2.6. Characterization of the TCNs-pDNA complex

Using photon correlation spectroscopy and Dynamic light scattering (DLS), the average particle size of the TCNs-pDNA complex was ascertained. Using a Zetasizer Nano ZS device (Malvern Instruments Ltd., Malvern & Worcestershire, UK), the measurements were carried out at 25℃. Using the same device, the zeta potential of the TCNs-pDNA complex dispersion was determined by electrophoretic mobility at 25℃. For each particle size and zeta potential tested, all samples were diluted 20-fold in water before being analyzed [27].

2.7. Cell culture, in vitro *transfection study*

The culture media for HEK293 and GTM3 cells included 10% FBS, 100 units/mL of penicillin, and 100 μg/mL of streptomycin. In 25 cm^2 polystyrene tissue culture flasks, cells were cultured at 37℃ in a humidified environment with 5% CO_2. The cells were cultured overnight to approximately 70% confluence after being seeded at a density of 3×10^5 cells/well on 24-well sterile culture plates. After removing the media the next day, cells were given two washes in preheated phosphate-buffered saline (PBS) before the addition of new serum-free DMEM medium [28–30].

Cells were cultured for six hours after TCNs-pDNA with various N/P ratios (2:1, 5:1, and 10:1) and introduced to the wells at a concentration of 5 μg plasmid/well. The cells were treated with Lipofectamine 3000™, which was used as a control in serum-free DMEM (pDNA 800 ng/3.0 μL Lipofectamine 3000™ per well). Six hours later, DMEM supplemented with 10% FBS was added to the serum-free medium, and it was incubated for an additional 48 hours at 37°C in a humidified environment with 5% CO_2. Transfection efficiency was assessed by fluorescence microscopy. GFP-positive cells were counted manually from fluorescence microscopy images (40× magnification). For each well, five randomly selected fields of view were analyzed, and the percentage of transfected cells was calculated by averaging across these fields [31].

2.8. Cas9-GFP expression plasmid transfection with TCNs

The plasmid pSpCas9(BB)-2A-GFP, which fused 2A-GFP to Cas9 to enable the detection of Cas9 expression in the transfected cells, was utilized to assess the wild-type Cas9 expression plasmid transfection efficiency of TCNs [13,32].

HEK293 and GTM3 cells were placed on cover slips in a 24-well plate at a density of 2×10^4 cells/well and grown for 24 hours in order to detect the GFP expression and intracellular distribution of transfection. The cells were transfected with TCNs/pSpCas9 (BB)-2A-GFP at a 5:1 ratio and 5 μg plasmid/well after being plated at 5×10^4 cells/well in a 24-well plate. After 48 hours, cells were fixed for 15 minutes at room temperature using 4% paraformaldehyde (pH 7.4 in PBS). Cells were

counterstained with DAPI to stain nuclei. Fluoromount™ Aqueous Mounting Medium was used to mount the slides, and confocal laser scanning microscopy (CLSM, Zeiss-700) with a 20x objective was used to view the slides [33–35].

2.9. T7 Endonuclease 1 assay

Forty-eight hours after TCN–Cas9/sgRNA (MYOC) was delivered, genomic DNA was isolated from HEK293 cells and subjected to T7 Endonuclease 1 (T7E1) analysis. The CRISPR/Cas9 system was designed to target the MYOC gene using the sgRNA sequence 5′-GTTCTTCTGTGCACGTTGC-3′ adjacent to a PAM (NGG) motif [36,37]. Genomic DNA from transfected cells was PCR-amplified at the MYOC nuclease target site using forward primer (MYOC_F: 5′-GTTCTTCTGTGCACGTTGC-3′) and reverse primer (MYOC_R: 5′-CTGGTCCAAGGTCAATTGGT-3′) in 25 µL reactions containing high-fidelity DNA polymerase (manufacturer and catalog number). The PCR was performed under the following conditions: Initial denaturation at 95°C for 3 min; 35 cycles of denaturation at 95°C for 30 s, annealing at 58°C for 30 s, and extension at 72°C for 30 s; followed by a final extension at 72°C for 5 min, yielding an amplicon of approximately 420 bp. Amplicons were denatured and re-annealed (95°C for 5 min, ramped down to 25°C at −0.1°C/s) to generate heteroduplex DNA, which was then digested with 1 µL T7E1 (10 U/µL, New England Biolabs) in 20 µL cleavage reactions containing 1× NEBuffer 2 and 200 ng purified DNA for 15 min at 37°C. The digested products were resolved on 2%–3% agarose gel, and band intensities were quantified to estimate the indel frequency [38,39].

2.10. Statistical analysis

All experiments were performed at least in triplicate unless otherwise specified. Data are presented as mean ± standard deviation (SD). Statistical analyses were performed using GraphPad Prism (version X; GraphPad Software, San Diego, CA, USA). Particle size, zeta potential, and transfection efficiency data were analyzed using one-way analysis of variance (ANOVA) followed by Tukey's post hoc test for multiple comparisons. A p-value < 0.05 was considered statistically significant.

3. Results and discussion

3.1. Preparation of nanocarriers and complex formations with plasmid DNA

The succinic anhydride esterification process successfully activated the carboxylic acid moieties of TPGS, enabling covalent attachment to the amino groups of chitosan through amide bond formation (Figure 1). The resulting modified chitosan co-polymers, prepared with two different degrees of TPGS grafting, were expected to offer a biocompatible platform for enhancing the therapeutic efficacy of drugs with limited permeability, consistent with previous findings [18,40]. This structural modification not only improved solubility and stability but also enhanced the potential of chitosan-based carriers for nucleic acid delivery.

Beyond *in vitro* validation, the translational applicability of TCNs depends largely on their feasibility for large-scale production. The polyelectrolyte complex coacervation method employed in

this study demonstrated distinct advantages, being simple, cost-effective, and adaptable to industrial processes. Earlier studies have confirmed the reproducibility of this method for nanoparticle fabrication, and our preliminary scale-up experiments (data not shown) further supported these observations. TCNs maintained consistent particle size distribution and surface charge, with batch-to-batch variation below 5%, underscoring the robustness of the process. These findings suggested that TCNs can be manufactured in a scalable and reproducible manner, which is essential for advancing them toward clinical translation.

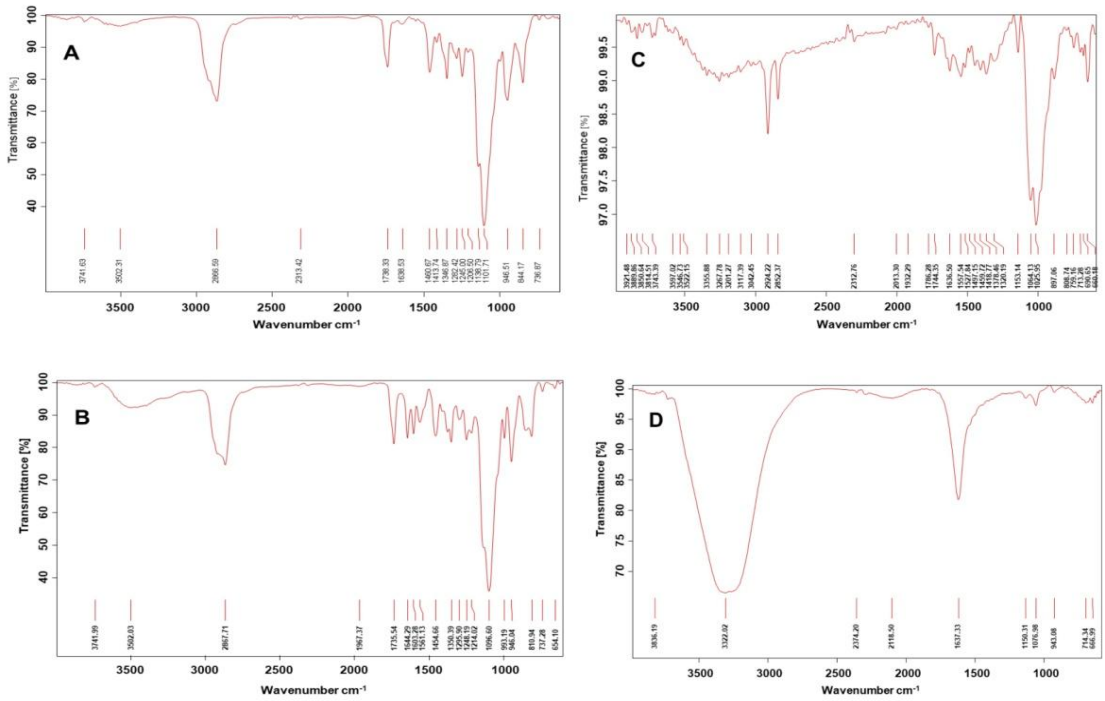

Figure 2. FTIR pattern of TPGS, TPGS-COOH, Chitosan, and TCNs.(A) TPGS characteristic bands alkyl-CH stretching (2866.59 cm^{-1}), -C=O stretching vibration (1738.33 cm^{-1}), OH group (3502.31 cm^{-1}), PEG chain's $–CH_2$ group (1346.87 cm^{-1}) are observed; (B) –C=O stretching vibration (1735.54 cm^{-1}), indicating that the TPGS activation (TPGS-COOH) had been effectively synthesized; (C) Characteristics bands of chitosan are observed for hydroxyl (-OH) stretching (3546.73 cm^{-1}) and the $-NH_2$ group band (3355.88 cm^{-1}); and (D) The amide (-CO-NH-) stretching (1637.33 cm^{-1}) band confirms the establishment between the carboxyl function of TPGS-COOH and the amine functional group of chitosan to form TCNs.

3.2. FTIR analysis of TPGS, chitosan, TPGS-COOH, and TCNs

FTIR spectroscopy was used to identify the effectively synthesized TPGS-COOH and TCNs. TPGS's distinctive peak is visible in Figure 2A. In particular, the aliphatic portions of the molecule were responsible for the alkyl-CH stretching band seen at 2866.59 cm^{-1}. At 1738.33 cm^{-1}, the -C=O stretching vibration is seen, and at 3502.31 cm^{-1}, the final OH group is visible. The stretching peaks

of (-C-O-) are seen at 1101.71 and 1282.42 cm^{-1}. At 1460.67 cm^{-1}, the aromatic ring's stretching –C–C– peak is apparent. The PEG chain's –CH2 group has an odd peak at 1346.87 cm^{-1}.

Figure 2B shows the FTIR spectrum of TPGS-COOH. The presence of the methyl group is shown by the –C-H stretching vibration that is seen at 2867.71 cm^{-1}. At 1735.54 cm^{-1}, the strong –C=O stretching vibration is very visible, indicating that the TPGS activation (TPGS-COOH) has been effectively synthesized. At 3502.03 cm^{-1}, TPGS-COOH molecules with the terminal hydroxyl functional band are particularly visible. Because of the presence of hydroxyl (-OH) stretching, the precise peak band occurs at 3546.73 cm^{-1} in the chitosan spectral data (Figure 2C). At 3355.88 cm^{-1}, the -NH2 group band is seen. The C-H stretching band is seen at 2852.37 cm^{-1} and 2924.22 cm^{-1}. The vibrations of C-O stretching and -NH bending are observed at 1378.46 cm^{-1} and 1557.54 cm^{-1}, respectively. At 1153.14 and 1064.13 cm^{-1}, precise C-O-C stretching band vibrations are observed [17]. The amide (-CO-NH-) stretching vibrations appear at 1637.33 cm^{-1} in the TCNs spectra (Figure 2D). The acquired peak verifies the formation of a connection between the amine functional group of chitosan and the carboxyl function of TPGS-COOH.

3.3. Electrophoretic mobility and enzymatic digestion assays

An electrophoretic mobility assay was conducted to examine the mobility of TCN–plasmid complexes and unbound plasmid. The plasmid band, which shows the movement of free plasmid into the gel, is observed in lane 1 of the gel (Figure 3). The full complex formation of all free plasmids is indicated by the absence of free plasmid bands in lanes of TCNs-pDNA complexes (lanes 3,5,7) with ratios of 2:1, 5:1, and 10:1. The gel wells in these samples show the only staining. The capacity of the complexes to shield the pDNA from enzymatic digestion was demonstrated by electrophoresis analyses conducted following DNase I incubation [14]. The digestion of free pDNA was confirmed by gel electrophoresis following DNase I incubation; no bands are observed (Figure 3, lane 2). In contrast, TCN–pDNA complexes resisted DNase I degradation and remained visible in gel wells (Lanes 4,6,8), confirming protection of pDNA. It should be noted that this assay provides only qualitative evidence of DNA protection; quantitative analysis (e.g., qPCR) was not performed in this study.

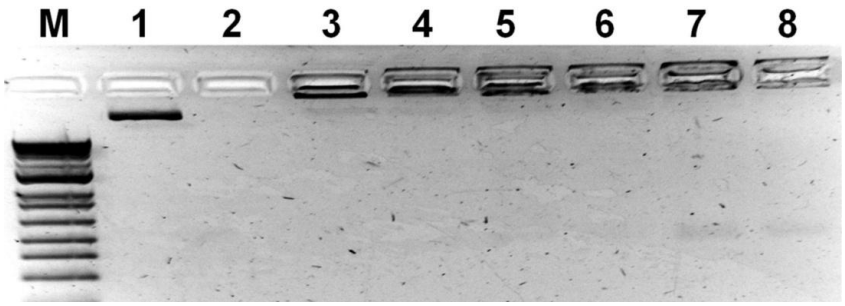

Figure 3. Agarose gel (1%) electrophoresis for DNase I protection assay. Lane M: DNA marker; Lane 1: Pre pGFP plasmid; Lane 2: pGFP plasmid digested with DNase I; Lanes 3, 5, and 7: TCN–plasmid (pDNA/pGFP) complexes at N/P ratios of 2:1, 5:1, and 10:1, respectively; and Lanes 4, 6, and 8: DNase I–digested TCN–plasmid (pDNA/pGFP) complexes at the same ratios. Note: pDNA and pGFP are used interchangeably in this study to refer to the same GFP-expressing plasmid.

The protective effect of TCNs against DNase I degradation is primarily attributed to electrostatic interactions between the positively charged amino groups of chitosan and the negatively charged phosphate backbone of DNA. This strong electrostatic attraction results in DNA condensation, effectively shielding it from nuclease attacks. The high zeta potential (> +20 mV) observed in our complexes reflects a sufficient cationic charge density that promotes stable condensation. In addition, steric hindrance arising from the nanocapsule matrix may further limit enzymatic access to the condensed DNA. Together, these mechanisms explain the observed resistance of TCNs–DNA complexes to nuclease degradation.

3.4. Characterization of TCNs-pDNA complexes

A variety of TCN–pDNA complex ratios (2:1, 5:1, and 10:1) were subjected to particle size analysis using DLS. The average particle sizes were 234 nm, 239 nm, and 248 nm for the 2:1, 5:1, and 10:1 ratios, respectively. Thus, all complexes remained in the sub-250 nm range, suitable for cellular uptake. Figure 4A presents a representative DLS profile for the optimized 5:1 ratio, which showed a Z-average size of 239 nm with a unimodal distribution. The same complexes were also analyzed for zeta potential, which remained above +20 mV across all ratios, indicating stable condensation of pDNA with TCNs. Figure 4B shows the representative zeta potential distribution for the 5:1 ratio (mean +22.7 mV).

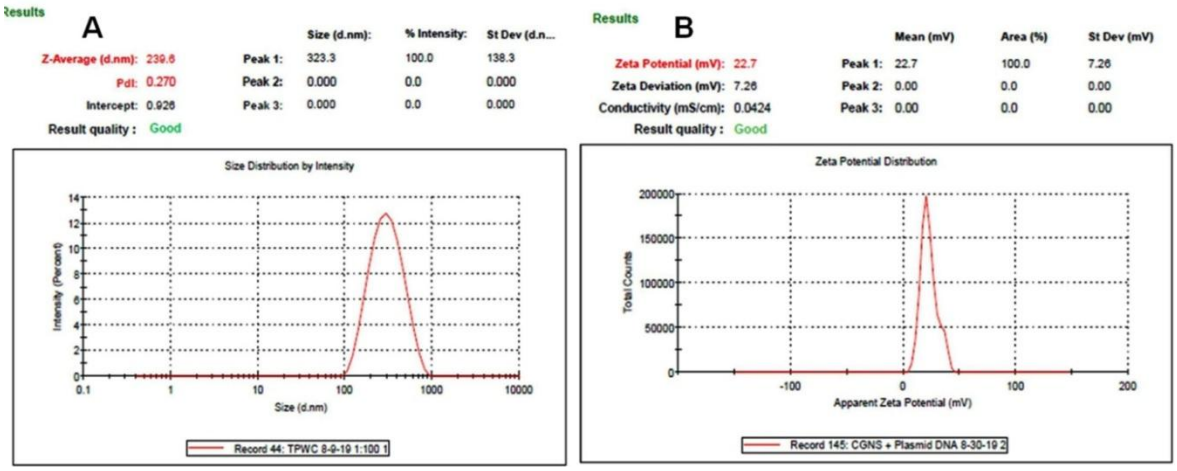

Figure 4. Characterization of TCN–pDNA complexes at the optimized N/P ratio of 5:1. (A) Dynamic light scattering (DLS) analysis showing average particle size distribution (Z-average: 239 nm; single peak at 323 nm). (B) Zeta potential distribution of the same complexes (mean +22.7 mV).

3.5. Cell culture transfection study

To determine transfection efficiencies of the TCNs for pDNA, we employed the eGFP reporter gene. Transfection efficiency of TCNs-pDNA complexes in HEK293 and GTM3 cells followed the order 5:1 > 10:1 > 2:1. Stable TCN–pDNA complexes were formed and used to transfect cells with high efficiency in vitro (Figure 5).

At the optimized N/P ratio of 5:1, transfection efficiencies reached approximately 90% in HEK293 cells and 81% in GTM3 cells. These values were obtained by manual counting of GFP-positive cells using fluorescence microscopy. In both cell lines, the transfection efficacy of TCNs-pDNA complexes at the 5:1 ratio was nearly identical to that of Lipofectamine 3000™.

Statistical analysis confirmed that TCNs at the 5:1 ratio achieved efficiencies not significantly different from Lipofectamine 3000™ ($p > 0.05$), whereas complexes at 2:1 and 10:1 ratio were significantly lower ($p < 0.05$). These findings support the potential of TCNs as a safe and effective non-viral vector formulation for ocular gene delivery.

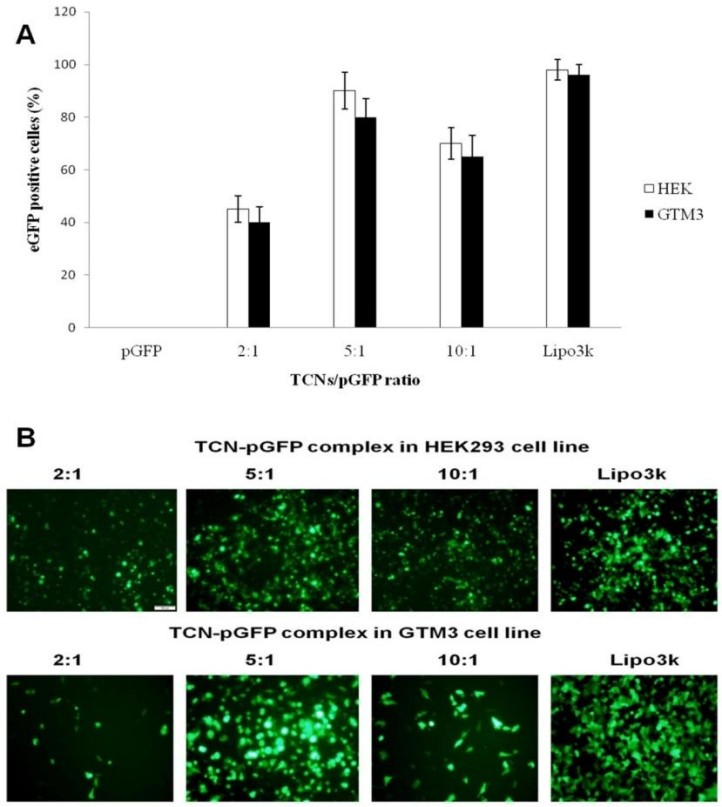

Figure 5. Transfection efficiency of TCNs in HEK293 and GTM3 culture cells at 24 h post-transfection. (A) Percentage of GFP-positive cells determined by manual counting under fluorescence microscopy at 40× magnification. TCN–pGFP complexes were tested at N/P ratios of 2:1, 5:1, and 10:1, and compared with Lipofectamine 3000™ (positive control). At the optimized 5:1 ratio, transfection efficiency was comparable to Lipofectamine 3000™. (B) Representative fluorescence microscopy images of HEK293 and GTM3 cells transfected with TCN–pGFP complexes at N/P ratios of 2:1, 5:1, and 10:1, and Lipofectamine 3000™ (positive control). Scale bar = 50 μm (magnification 40×).

3.6. Cas9-GFP expression plasmids transfection with TCNs

To make it easier to detect Cas9 expression in the transfected cells, the plasmid pSpCas9(BB)-2A-GFP, also known as px458, was utilized. This plasmid combines the reporter gene

GFP with the Cas9 expression cassette. Both HEK293 and GTM3 cells show transfection efficiency with TCNs+pSpCas9-GFP (Figure 6). To differentiate between intracellular and surface-localized TCNs+pSpCas9-GFP, Confocal Laser Scanning Microscopy (CLSM, Zeiss-700) observation was performed. Images of cellular uptake at 24 h are shown in Figure 6. The intracellular fluorescent signal from TCNs+pSpCas9-GFP is green and that of nuclei is blue.

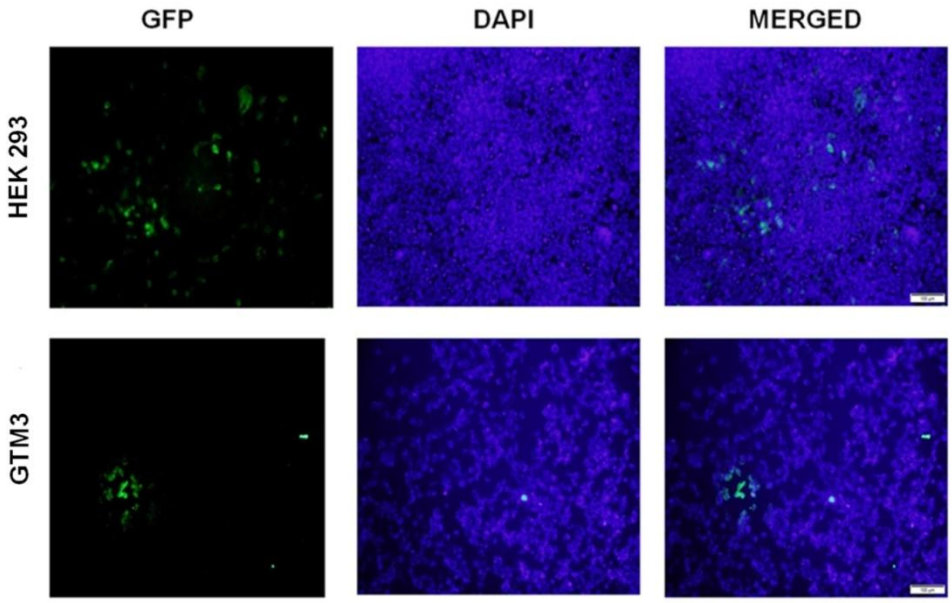

Figure 6. Cellular uptake of TCNs labeled with Cas9-GFP.Confocal Laser Scanning Microscopy (CLSM) images showing cellular uptake and expression of the TCN–pCas9–GFP complex after 24 h incubation with HEK and GTM3 cells. The images are the projection of x-y sections. TCNs were labeled with Cas9-GFP (green), and cell nuclei were stained with DAPI (blue). Magnification: × 10.

3.7. T7 endonuclease I assay

The CRISPR/Cas9 system introduces targeted double-strand breaks at specific genomic loci through the guidance of a single guide RNA (sgRNA) [41]. Cas9 recognizes protospacer adjacent motif (PAM) sequences in the DNA and cleaves at the complementary sgRNA-binding site. DNA breaks are subsequently repaired by the non-homologous end joining (NHEJ) pathway, often resulting in insertions or deletions (INDELs). These INDELs create mismatches (heteroduplexes) when PCR products spanning the target site are denatured and re-annealed, which can then be recognized and cleaved by T7 endonuclease I.

To assess MYOC gene editing *in vitro*, genomic DNA was isolated from HEK293 cells treated with TCN–Cas9/sgRNA (MYOC). The target MYOC locus was amplified by PCR, and the amplicons were denatured and re-annealed to enable heteroduplex formation. Subsequent digestion with T7 endonuclease I revealed cleavage products, confirming the presence of CRISPR/Cas9-induced INDEL mutations (Figure 7). Compared with untreated negative controls, TCN–Cas9/sgRNA (MYOC)–treated cells showed distinct cleavage bands, demonstrating efficient MYOC gene disruption mediated by the TCN delivery system.

Although we demonstrated robust *in vitro* efficacy of TCNs for CRISPR/Cas9-mediated *MYOC* gene editing, future work is needed to validate their therapeutic potential in vivo. One limitation of the current study is that DNA protection against DNase I was assessed only qualitatively using agarose gel electrophoresis. Quantitative qPCR analysis was not performed; however, we recognize this as an important next step and recommend it as a future validation to determine the precise extent of plasmid retention following nuclease challenge. Given the established safety of chitosan and TPGS, we anticipate favorable tolerance in ocular tissues. For clinical translation, TCNs could be adapted for topical administration (eye drops) or intracameral injection, both of which are minimally invasive and suitable for glaucoma therapy. These studies will be essential to establish the long-term safety and therapeutic viability of TCN-mediated non-viral gene delivery for myocilin-associated glaucoma.

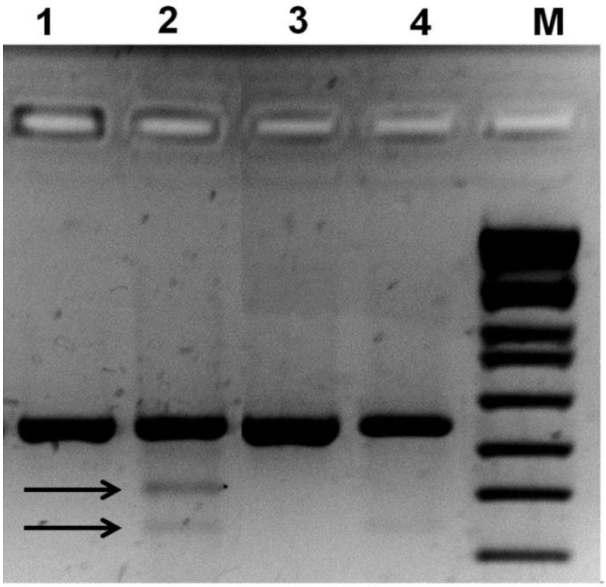

Figure 7. T7 Endonuclease I assay of MYOC gene editing in HEK293 cells. Genomic DNA was PCR-amplified at the MYOC target locus (~420 bp), re-annealed to form heteroduplexes, and digested with T7 endonuclease I. Lane M: DNA marker (100 bp ladder; major bands indicated at 100, 200, 300, 400, and 500 bp). Lane 1: TCNs–Cas9 only (uncut PCR product, ~420 bp). Lane 2: TCN–Cas9/sgRNA (MYOC), showing cleavage bands at ~280 bp and ~140 bp in addition to the full-length band, confirming INDEL formation. Lanes 3–4: untreated negative controls, showing intact ~420 bp PCR product. A faint low-molecular-weight band in lane 4 is attributed to nonspecific PCR byproducts and does not indicate editing.

4. Conclusions

In this study, we developed positively charged D-α-tocopheryl glycol succinate 1000 (TPGS)-chitosan nanocapsules as a non-viral vector for plasmid delivery in genome editing applications. Cationic TPGS–chitosan nanocapsules (TCNs) were synthesized through a two-step reaction involving functionalization of TPGS with succinic anhydride followed by ionic crosslinking with chitosan via a complex coacervation method. FTIR spectroscopy confirmed successful

conjugation of TPGS and chitosan. DNase protection assays demonstrated that plasmid DNA complexed with TCNs was shielded from enzymatic degradation. The nanocapsules showed particle sizes below 250 nm and zeta potentials above +20 mV. Transfection efficiency at an N/P ratio of 5:1 was comparable to Lipofectamine 3000™ in both HEK293 and GTM3 cells. Transfection of both HEK293 and GTM3 cells was achieved using TCNs+Cas9-GFP. Furthermore, T7E1 assays indicated successful targeting of the *MYOC* locus in HEK293 cells. Taken together, these findings provide proof-of-concept for TCNs as a promising non-viral nanocarrier system for future CRISPR/Cas9-based gene therapy applications in glaucoma.

Author contributions

KK: Conceptualization, Methodology, investigation, writing-Original Draft preparation. **VK**: Writing- Original draft preparation. **JR**: Writing - Review & Editing. **CS**: Investigation. **VCS**: Conceptualization, Validation, Supervision.

Use of Generative-AI tools declaration

No generative artificial intelligence (AI) tools were used in the preparation, writing, or editing of this manuscript. All content is entirely the work of the authors.

Acknowledgments

Research was supported by Department of Biotechnology (DBT) along with Indo U.S. Science & Technology Forum (IUSSTF), New Delhi, India, in terms of Overseas Fellowship of Genome Engineering/Editing Technology Initiative Program. This research was funded by DBT and IUSSTF, Award Letter No Indo-US GET in Overseas Fellowship 2019-0109/Kesavan Kathikeyan dated 19th June 2019 (KK). This work was also supported by NIH P30EY025580 (VCS).

Conflict of interest

The authors declare no conflicts of interest in this paper.

References

1. Morthen MK, Magno MS, Utheim TP, et al. (2022) The vision-related burden of dry eye, *Ocul Surf* 23: 207–215. https://doi.org/10.1016/j.jtos.2021.10.007
2. Solinís MÁ, del Pozo-Rodríguez A, Apaolaza PS, et al. (2015) Treatment of ocular disorders by gene therapy. *Eur J Pharm Biopharm* 95: 331–342.https://doi.org/10.1016/j.ejpb.2014.12.022
3. Naik R, Mukhopadhyay A, Ganguli M (2009) Gene delivery to the retina: Focus on non-viral approaches. *Drug Discov Today* 14: 306–315. https://doi.org/10.1016/j.drudis.2008.09.012
4. Alqawlaq S, Sivak JM, Huzil JT, et al. (2014) Preclinical development and ocular biodistribution of gemini-DNA nanoparticles after intravitreal and topical administration: Towards non-invasive glaucoma gene therapy. *Nanomed-Nanotechnol* 10: 1637–1647. https://doi.org/10.1016/j.nano.2014.05.010

5. DiCarlo JE, Sengillo JD, Justus S, et al. (2017) CRISPR-Cas genome surgery in ophthalmology. *Transl Vis Sci Techn* 6: 13. https://doi.org/10.1167/tvst.6.3.13
6. Li L, Hu S, Chen X. (2018) Non-viral delivery systems for CRISPR/Cas9-based genome editing: Challenges and opportunities. *Biomaterials* 171: 207–218. https://doi.org/10.1016/j.biomaterials.2018.04.031
7. Li L, He ZY, Wei XW, et al. (2015) Challenges in CRISPR/Cas9 delivery: Potential roles of nonviral vectors. *Hum Gene Ther* 26: 452–462. https://doi.org/10.1089/hum.2015.069
8. Kesavan K, Mohan P, Gautam N, et al. (2020) Topical ocular delivery of nanocarriers: A feasible choice for glaucoma management. *Curr Pharm Des* 26: 5518–5532. https://doi.org/10.2174/1381612826666200916145609
9. Yin H, Kanasty RL, Eltoukhy AA, et al. (2014) Non-viral vectors for gene-based therapy. *Nat Rev Genet* 15: 541–555. https://doi.org/10.1038/nrg3763
10. Jain A, Zode G, Kasetti RB, et al. (2017) CRISPR-Cas9-based treatment of myocilin-associated glaucoma. *Proc Natl Acad Sci USA* 114: 11199–11204. https://doi.org/10.1073/pnas.1706193114
11. Aghmiuni AI, Keshel SH, Rahmani A, et al. (2023) Retinal tissue engineering: Regenerative and drug delivery approaches. *Curr Stem Cell Res Ther* 18: 608–640. https://doi.org/10.2174/1574888X17666220621153508
12. Oliveira AC, Martens TF, Raemdonck K, et al. (2014) Dioctadecyldimethylammonium: Monoolein nanocarriers for efficient in vitro gene silencing. *ACS Appl Mater Interfaces* 6: 6977–6989. https://doi.org/10.1021/am500793y
13. Wang HX, Song Z, Lao YH, et al. (2018) Nonviral gene editing via CRISPR/Cas9 delivery by membrane-disruptive and endosomolytic helical polypeptide. *Proc Natl Acad Sci USA* 115: 4903–4908. https://doi.org/10.1073/pnas.1712963115
14. Bordelon H, Biris AS, Sabliov CM, et al. (2011) Characterization of plasmid DNA location within chitosan/PLGA/pDNA nanoparticle complexes designed for gene delivery. *J Nanomater* 952060. https://doi.org/10.1155/2011/952060
15. Bozkir A, Saka OM (2004) Chitosan-DNA nanoparticles: Effect on DNA integrity, bacterial transformation and transfection efficiency. *J Drug Target* 12: 281–288. https://doi.org/10.1080/10611860410001714162
16. Puras G, Mashal M, Zárate J, et al. (2014) A novel cationic niosome formulation for gene delivery to the retina. *J Control Release* 174: 27–36. https://doi.org/10.1016/j.jconrel.2013.11.004
17. Mohan P, Rajeswari J, Kesavan K (2023) TPGS-chitosan conjugated mucoadhesive micelles of brinzolamide for glaucoma therapy: *In vitro* and *in vivo* evaluation. *Materialia* 28: 101711. https://doi.org/10.1016/j.mtla.2023.101711
18. Mohyeldin SM, Samy WM, Ragab D, et al. (2021) Hybrid lipid core chitosan-TPGS shell nanocomposites as a promising integrated nanoplatform for enhanced oral delivery of sulpiride in depressive disorder therapy. *Int J Biol Macromol* 188: 432–449. https://doi.org/10.1016/j.ijbiomac.2021.08.035
19. Mohan P, Kesavan K. (2021) Cationic polyelectrolyte nanocapsules of moxifloxacin for microbial keratitis therapy: Development, characterization, and pharmacodynamic study. *AAPS Pharm Sci Tech* 22:195. https://doi.org/10.1208/s12249-021-02039-1

20. Peng E, Ding J, Xue JM (2012) Succinic anhydride functionalized alkenoic ligands: A facile route to synthesize water dispersible nanocrystals. *J Mater Chem* 22: 13832–12840. https://doi.org/10.1039/C2JM30942D
21. Martien R, Loretz B, Thaler M, et al. (2007) Chitosan–thioglycolic acid conjugate: An alternative carrier for oral nonviral gene delivery? *J Biomed Mater Res A* 82: 1–9. https://doi.org/10.1002/jbm.a.31135
22. Lueckheide M, Vieregg JR, Bologna AJ, et al. (2018) Structure-property relationships of oligonucleotide polyelectrolyte complex micelles. *Nano Lett* 18: 7111–7117. https://doi.org/10.1021/acs.nanolett.8b03132
23. Amine S, Montembault A, Fumagalli M, et al. (2021) Controlled polyelectrolyte association of chitosan and carboxylatednano-fibrillated cellulose by desalting. *Polymers* 13: 2023. https://doi.org/10.3390/polym13122023
24. Zhao M, Zacharia NS (2018) Protein encapsulation via polyelectrolyte complex coacervation: Protection against protein denaturation. *J Chem Phys* 149: 163326. https://doi.org/10.1063/1.5040346
25. Bearden JC (1979) Electrophoretic mobility of high-molecular-weight, double-stranded DNA on agarose gels. *Gene* 6: 221–234. https://doi.org/10.1016/0378-1119(79)90059-3
26. Hu Y, Xu BH, Xu JJ, et al. (2014) Synthesis of mannosylatedpolyethylenimine and its potential application as cell-targeting non-viral vector for gene therapy. *Polymers* 6: 2573–2587. https://doi.org/10.3390/polym6102573
27. Malm AV, Corbett JCW (2019) Improved Dynamic Light Scattering using an adaptive and statistically driven time resolved treatment of correlation data. *Sci Rep* 9:13519. https://doi.org/10.1038/s41598-019-50077-4
28. Tan E, Chin CSH, Lim ZFS, et al. (2021) HEK293 cell line as a platform to produce recombinant proteins and viral vectors. *Front Bioeng Biotechnol* 9: 796991. https://doi.org/10.3389/fbioe.2021.796991
29. Helms HC, Abbott NJ, Burek M, et al. (2016) Invitro models of the blood-brain barrier: An overview of commonly used brain endothelial cell culture models and guidelines for their use. *J Cereb Blood F Met* 36: 862–890. https://doi.org/10.1177/0271678X16630991
30. Bae DH, Marino M, Iaffaldano B, et al. (2020) Design and testing of vector-producing HEK293T cells bearing a genomic deletion of the SV40T antigen coding region. *Mol Ther Methods Clin Dev* 18: 631–638. https://doi.org/10.1016/j.omtm.2020.07.006
31. Jin Y, Wang S, Tong L, et al. (2015) Rational design of didodecyldimethylammonium bromide-based nanoassemblies for gene delivery. *Colloid Surface B* 126: 257–264. https://doi.org/10.1016/j.colsurfb.2014.12.032
32. Patil SV, Kaipa BR, Ranshing S, et al. (2024) Lentiviral mediated delivery of CRISPR/Cas9 reduces intraocular pressure in a mouse model of myocilin glaucoma. *Sci Rep* 14: 6958. https://doi.org/10.1038/s41598-024-57286-6
33. Mori Y, Yoshida Y, Satoh A, et al. (2020) Development of an experimental method of systematically estimating protein expression limits in HEK293 cells. *Sci Rep* 10: 4798. https://doi.org/10.1038/s41598-020-61646-3
34. Hart T, Tong AHY, Chan K, et al. (2017) Evaluation and design of genome-wide CRISPR/SpCas9 knockout screens. *G3* 7: 2719–2727. https://doi.org/10.1534/g3.117.041277

35. Li K, Wang G, Andersen T, et al. (2014) Optimization of genome engineering approaches with the CRISPR/Cas9 system. *PLoS One* 9: e105779. https://doi.org/10.1371/journal.pone.0105779
36. Soh CL, Huangfu D (2017) CRISPR/Cas9-mediated mutagenesis of human pluripotent stem cells in defined Xeno-free E8 medium. In: *In Vitro Mutagenesis*. New York: Humana Press. 1498: 57–78. https://doi.org/10.1007/978-1-4939-6472-7_5
37. González-Romero E, Martínez-Valiente C, García-García G, et al. (2023) PCR-based strategy for introducing CRISPR/Cas9 machinery into hematopoietic cell lines. *Cancers* 15: 4263. https://doi.org/10.3390/cancers15174263
38. Petrova IO, Smirnikhina SA (2023) The development, optimization and future of prime editing. *Int J Mol Sci* 24: 17045. https://doi.org/10.3390/ijms242317045
39. Shi Y, Tan Q, Yang C, et al. (2024) Establishment of a cleavage-based single-plasmid dual-luciferase surrogate reporter for the cleavage efficiency evaluation of CRISPR-Cas12a systems and its primary application. *CRISPR J* 7: 156–167. https://doi.org/10.1089/crispr.2024.0038
40. Luo J, Tan G, Thong KX, et al. (2022) Non-viralgene therapy in trabecular meshwork cells to prevent fibrosis in minimally invasive glaucoma surgery. *Pharmaceutics* 14: 2472. https://doi.org/10.3390/pharmaceutics14112472
41. Alonso-Lerma B, Jabalera Y, Samperio S, et al. (2023) Evolution of CRISPR-associated endonucleases as inferred from resurrected proteins. *Nat Microbiol* 8: 77–90. https://doi.org/10.1038/s41564-022-01265-y

AIMS Press